ACT/FHS System Identification Including Rotor and Engine Dynamics

Susanne Seher-Weiß

Research Scientist
DLR (German Aerospace Center)
Braunschweig, Germany

ABSTRACT

At the DLR Institute of Flight Systems models of the ACT/FHS, an EC135 with a fly-by-wire/light flight control system, are needed for control law development and simulation. Thus, models are sought that cover the whole flight envelope and are valid over a broad range of frequencies. Furthermore, if the models are to be used in the feedforward loop of the model following control system, they have to be invertible and thus must not have any positive transmission zeros. Maximum likelihood system identification in the frequency domain was used to derive the desired models. For rotor flapping the explicit formulation with flapping angles was modified slightly to avoid positive transmission zeros. For the regressive lead-lag a simple model formulation was found that needs only one dipole with two states. The engine dynamics were first modeled separately and then coupled to the body/rotor model. The final integrated model has seventeen states and yields a good match for frequencies up to 30 rad/s.

NOMENCLATURE	
a,b	flapping angles, rad
$A_{},B_{}$	flapping angle derivatives
a_x, a_y, a_z	body-fixed linear accelerations, m/s ²
c	rotor blade chord, m
$C_{L_{\alpha}}$	blade lift curve slope, 1/rad
$C_T^{-\alpha}$	thrust coefficient, $C_T = T/[\rho \pi R^2 (\Omega R)^2]$
C_0	inflow constant
$D_{\delta_{lon}}, D_{\delta_{lat}}$	control derivatives of the lead-lag dipole
e^{-ion}	hinge offset, m
$E_{}$	engine model parameters
g	acceleration of gravity, m/s ²
I_{eta}	blade flapping moment of inertia, kg m ²
K_{eta}	flapping stiffness, Nm/rad
K_{θ_0}	control gain, rad/%
$L_{}, M, N$	moment derivatives
m	aircraft mass, kg
p,q,r	roll, pitch and yaw rates, rad/s
Q	engine torque, Nm
R	rotor radius, m
T	rotor thrust, N
u, v, w	body-fixed velocity components, m/s
x_i, y_i, z_i	canonical dipole states, $i = 1, 2$
$X_{},Y,Z$	force derivatives
$oldsymbol{eta}_0$	coning angle, rad
$\delta_{lon}, \delta_{lat}$	longitudinal, lateral cyclic inputs, %
$\delta_{ped}, \delta_{col}$	pedal and collective inputs, %
ε	hinge offset ratio, $\varepsilon = e/R$
Φ,Θ	roll and pitch angles, rad
γ	Lock number, $\gamma = \rho C_{L_{\alpha}} c R^4 / I_{\beta}$

NOMENICI ATTIDE

Presented at the AHS International 73rd Annual Forum & Technology Display, Fort Worth, Texas, USA, May 9–11, 2017. Copyright © 2017 by AHS International, Inc. All rights reserved.

γ^*	effective Lock number,
	$\gamma^* = \gamma/(1 + C_{L_{lpha}}\sigma/(16ar{v}_0))$
ν	inflow, m/s
$ar{v}_0$	trim inflow ratio, $\bar{\mathbf{v}}_0 = \sqrt{C_{T_0}/2}$
ρ	air density, kg/m ³
σ	solidity
au	time delay, s
$ au_f$	flapping time constant, s
$rac{ au_f}{\zeta}$	damping
ω	frequency, rad/s
$[\zeta, \omega]$	short for $s^2 + 2\zeta\omega + \omega^2$
Ω	rotor speed, rad/s
Indices	
0	trim value
en	engine
ll	lead-lag
Acronyms	
ACT/FHS	Active Control Technology / Flying Helicopter
	Simulator
DLR	German Aerospace Center
ML	maximum likelihood

INTRODUCTION

The German Aerospace Center (DLR) operates the ACT/FHS (Active Control Technology / Flying Helicopter Simulator, see Fig. 1) as a test bed for various research projects (Refs. 1–3). The ACT/FHS is based on a Eurocopter EC135, a light, twin-engine helicopter with a bearingless main rotor and a fenestron. Models of different complexity for the ACT/FHS are needed for simulation and control law development. Therefore, system identification for the ACT/FHS is an ongoing process with first results already presented in 2007 (Ref. 4).



Fig. 1. DLR research helicopter ACT/FHS

As models are sought for the whole flight envelope, dedicated flight tests with sweep and multistep inputs in all controls have been performed at five reference speeds (hover, 30, 60, 90, 120 knots) and yield the database for all system identification efforts. If models for the different reference speeds are to be used as a basis for a full flight envelope quasi-nonlinear simulation as described in (Ref. 5), they must have the same model structure to allow for interpolation (model stitching), see (Refs. 6, 7).

Models that are to be used in the feedforward loop of the model following control system (MFCS) (Refs. 2, 8, 9), must be invertible (see Fig. 2). Therefore, these models must not have any positive transmission zeros when reduced to the output variables to be matched (p, q, r, a_z) because positive transmission zeros would result in unstable poles in the inverted model.

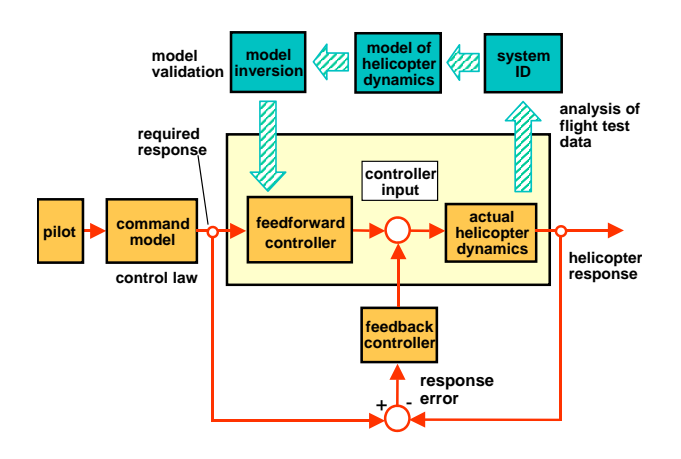


Fig. 2. MFCS general structure

Ideally, a model to be used for control law development should be accurate from one decade below to one decade above the cutoff frequency (\pm half a decade ist usually sufficient). For the ACT/FHS with a cutoff frequency of 3 rad/s in pitch and 5 rad/s in roll, this means that the models should accurately cover the frequency range of 0.5-30 rad/s. Therefore, an extended model structure is necessary that explicitly includes the regressive flapping, coupled inflow/coning, and regressive lead-lag states of the rotor.

In the past, different modeling aspects of ACT/FHS system identification have been described in separate papers (Refs. 10, 11). In this paper, these results are reevaluated with respect to the requirements of model interpolation and model inversion. Furthermore, results from investigations using the optimized predictor-based subspace identification (PBSIDopt) method (Ref. 12) are used to develop a simplified formulation for the influence of the regressive lead-lag. Also, this paper shows how deficits in yaw rate approximation are reduced by engine modeling.

The paper will first describe the modeling that was used for the different rotor degrees of freedom. Next, the development of a dynamic engine model and its integration into the overall model will be shown. Finally, some results for the fully integrated model will be presented.

FLAPPING

Rotor flapping is usually accounted for in system identification modeling with the explicit formulation developed by Tischler (Ref. 13). This explicit formulation includes two coupled first order differential equations for the longitudinal and lateral flapping angles a and b that are triggered by the longitudinal and lateral cyclic control inputs.

$$\tau_f \dot{a} = -a + A_b b + \tau_f q + A_{\delta_{lon}} \delta_{lon} + A_{\delta_{lat}} \delta_{lat}
\tau_f \dot{b} = -b + B_a a + \tau_f p + B_{\delta_{lon}} \delta_{lon} + B_{\delta_{lat}} \delta_{lat}$$
(1)

The flapping angles are coupled to the rigid-body equations via

$$\dot{u} = X_{u}u + X_{v}v + X_{w}w - w_{0}q + (X_{r} + v_{0})r$$

$$-g\cos\Theta_{0}\Theta + X_{a}a + X_{\delta_{col}}\delta_{col} + X_{\delta_{ped}}\delta_{ped}$$

$$\dot{v} = Y_{u}u + Y_{v}v + Y_{w}w + (Y_{p} + w_{0})p + (Y_{r} - u_{0})r$$

$$+g\cos\Theta_{0}\Phi + Y_{b}b + Y_{\delta_{col}}\delta_{col} + Y_{\delta_{ped}}\delta_{ped}$$

$$\dot{p} = L_{u}u + L_{v}v + L_{w}w + L_{r}r + L_{b}b$$

$$+L_{\delta_{col}}\delta_{col} + L_{\delta_{ped}}\delta_{ped}$$

$$\dot{q} = M_{u}u + M_{v}v + M_{w}w + M_{r}r + M_{a}a$$

$$+M_{\delta_{col}}\delta_{col} + M_{\delta_{ped}}\delta_{ped}$$

Compared to a standard 6-DoF model, the cyclic control derivatives $X_{\delta_{lon}}, X_{\delta_{lat}}, Y_{\delta_{lon}}, Y_{\delta_{lat}}, L_{\delta_{lon}}, L_{\delta_{lat}}, M_{\delta_{lon}}$, and $M_{\delta_{lat}}$ have been replaced by the corresponding control derivatives $A_{\delta_{lon}}, A_{\delta_{lat}}, B_{\delta_{lon}}$, and $B_{\delta_{lat}}$ in the equations of the flapping dynamics. Similarly, the standard force and moment derivatives $X_p, X_q, Y_q, L_p, L_q, M_p$, and M_q have been replaced by the rotor force and moment terms L_b, M_a, X_a , and Y_b that couple the main rotor to the fuselage. The quasi-static force derivative Y_p is often retained to account for tail rotor effects.

The force terms X_a , and Y_b are constrained due to physical considerations $Y_b = -X_a$. Their numerical value is theoretically equal to the acceleration of gravity g and therefore often constrained to this value for the identification.

$$X_a = -Y_b = g \tag{3}$$

A theoretical value for the rotor flap time constant τ_f can be calculated from the hinge offset e and the effective lock number γ^* ,

$$\frac{1}{\tau_f} = \frac{\gamma^* \Omega}{16} \left(1 - \frac{8e}{3R} \right) \tag{4}$$

but τ_f is usually left as a free parameter in the identification.

For the identification of the ACT/FHS, an implicit formulation of the flapping equations as first described in (Ref. 4) had been used that results in \dot{p} and \dot{q} as two additional state variables.

$$\ddot{p} = \hat{L}_{p}p + \hat{L}_{\dot{p}}\dot{p} + \hat{L}_{\delta_{lat}}\delta_{lat}
\ddot{q} = \hat{M}_{q}q + \hat{M}_{\dot{q}}\dot{q} + \hat{M}_{\delta_{lon}}\delta_{lon}$$
(5)

In (Ref. 10) it was shown that the explicit and the implicit formulation of the rotor flapping dynamics produce equivalent results.

The reason for using this implicit formulation was that for the ACT/FHS the explicit formulation led to models with positive transmission zeros that therefore could not be used for model following control.

On the other hand, it was expected that models with explicit flapping would be superior regarding interpolation between different reference speeds for model stitching (Ref. 5) due to better separation of the rigid-body and rotor degrees of freedom. Thus, it was tried to modify the explicit model formulation to solve the problem with the positive transmission zeros.

Let A_{ex} and B_{ex} be the system matrices of the explicit model

$$\dot{\mathbf{x}}_{ex} = \mathbf{A}_{ex}\mathbf{x}_{ex} + \mathbf{B}_{ex}\mathbf{u} \tag{6}$$

with a state vector of

$$\mathbf{x}_{ex}^{T} = [u, v, w, p, q, r, \Phi, \Theta, a, b]$$
(7)

and control inputs **u**. Then a transformation matrix **T** that consists of an 8x8 identity matrix I_8 , an 8x2 matrix of zeros $O_{8,2}$ and the rows of A_{ex} that correspond to q and p

$$\mathbf{T} = \begin{bmatrix} \mathbf{I}_8 & \mathbf{O}_{8,2} \\ \mathbf{A}_{ex}(5,:) \\ \mathbf{A}_{ex}(4,:) \end{bmatrix}$$
(8)

can be used to transform the system from eq. (6) via

$$\mathbf{A}_{im} = \mathbf{T}\mathbf{A}_{ex}\mathbf{T}^{-1}, \quad \mathbf{B}_{im} = \mathbf{T}\mathbf{B}_{ex} \tag{9}$$

into an implicit model

$$\dot{\mathbf{x}}_{im} = \mathbf{A}_{im}\mathbf{x}_{im} + \mathbf{B}_{im}\mathbf{u} \tag{10}$$

with a state vector of

$$\mathbf{x}_{im}^{T} = [u, v, w, p, q, r, \Phi, \Theta, \dot{q}, \dot{p}] \tag{11}$$

Transforming the models identified with the explicit flapping equations into the implicit formulation as just described and comparing the resulting matrices showed that the main differences were in the collective and pedal control derivatives. Therefore, the explicit formulation of rotor flapping was modified in such a way that the collective control input also acts on the flapping angles.

$$\tau_{f}\dot{a} = -a + A_{b}b + \tau_{f}q + A_{\delta_{lon}}\delta_{lon} + A_{\delta_{lat}}\delta_{lat} + A_{\delta_{col}}\delta_{col}
\tau_{f}\dot{b} = -b + B_{a}a + \tau_{f}p + B_{\delta_{lon}}\delta_{lon} + B_{\delta_{lat}}\delta_{lat} + B_{\delta_{col}}\delta_{col}
(12)$$

The corresponding quasi-static collective control derivatives L_{δ_0} and M_{δ_0} in the pitch and roll rate equations were dropped. This slight model modification led to models for the ACT/FHS without positive transmission zeros. The quasi-static pedal control derivatives could remain unchanged.

The match with this modified explicit flapping formulation is almost identical to the match achieved with the models with the implicit flapping formulation as can be seen from Fig. 3.

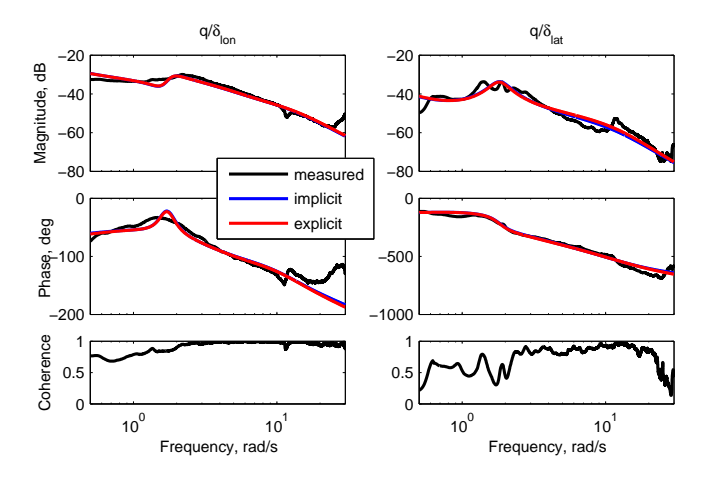


Fig. 3. Match in pitch rate for implicit and modified explicit flapping (60 kts)

INFLOW/CONING

Modeling of the inflow/coning dynamics is necessary to capture the rising amplitude in the frequency response for vertical acceleration due to collective input and can be achieved by different modeling approaches.

The approach most widely used for modeling the inflow/coning dynamics and their coupling to the fuselage is the hybrid formulation developed by Tischler (Ref. 13). It is based on the work by Chen and Hindson (Ref. 14) who developed analytical models for the coupled inflow/coning/heave dynamics.

The first-order inflow dynamics are written as

$$\dot{\mathbf{v}} = \frac{-75\pi\Omega}{32} \left(\bar{\mathbf{v}}_0 + \frac{C_{L\alpha}\sigma}{16} \right) C_0 \mathbf{v} + V_{\dot{\beta}_0} \dot{\beta}_0$$
$$+ \frac{25\pi\Omega^2 R}{32} \left(\frac{C_{L\alpha}\sigma}{8} \right) C_0 K_{\theta_0} \delta_{col} \tag{13}$$

with the trim inflow ratio \bar{v}_0 and thrust coefficient C_{T_0} using $T_0 = mg$ for the trim thrust. The control gain K_{θ_0} transforms collective input to effective blade root pitch angle (θ_0) .

For hovering flight, an analytical expression is available for $V_{\dot{eta_0}}$

$$V_{\dot{\beta_0}} = \frac{-25\pi\Omega R}{32} \quad \bar{v}_0 + \frac{C_{L\alpha}\sigma}{8} \quad C_0$$
 (14)

The rigid-blade coning dynamics, ignoring the influence of hinge offset and flapping spring, are expressed as a secondorder differential equation

$$\ddot{\beta}_0 = -\frac{\Omega \gamma}{8} \dot{\beta}_0 - \Omega^2 \beta_0 - \frac{\Omega \gamma}{6R} v + \frac{\Omega^2 \gamma}{8} K_{\theta_0} \delta_{col}$$
 (15)

resulting in two states, coning angle β_0 and coning rate $\dot{\beta}_0$.

Finally, the coning/inflow dynamics are coupled to the fuselage through the thrust coefficient C_T , to achieve the hybrid model structure for the vertical dynamics

$$\dot{w} = Z_u u + Z_v v + Z_w w + (Z_p - v_0) p + (Z_q + u_0) q + Z_r r$$

$$-g \cos \Phi_0 \sin \Theta_0 \Theta - \frac{\rho \pi R^2 (\Omega R)^2}{m} C_T$$

$$+ Z_{\delta_{lon}} \delta_{lon} + Z_{\delta_{lat}} \delta_{lat} + Z_{\delta_{ned}} \delta_{ped}$$

$$(16)$$

where the perturbation thrust coefficient C_T is given by

$$C_T = \frac{0.543}{\Omega^2 R} \frac{1}{C_0} \dot{\mathbf{v}} + \frac{4\bar{\mathbf{v}}_0}{\Omega R} \mathbf{v} + \frac{4\bar{\mathbf{v}}_0}{3\Omega} \dot{\boldsymbol{\beta}}_0 \tag{17}$$

The quasi-steady collective control force derivative $Z_{\delta_{col}}$ is missing in eq. (16) for the vertical acceleration because the control path is now changed: Collective control inputs cause an increase in blade angle of attack that increases inflow and coning (see eqs. (13) and (15)). The corresponding dynamic variations in thrust from eq. (17) are transmitted to the fuse-lage via eq. (16) resulting in a change of vertical acceleration.

The inflow constant C_0 in eqs. (13) and (17) allows for the selection of either the Carpenter-Fridovich theory inflow time constant ($C_0 = 0.639$) or the Pitt-Peters time constant ($C_0 = 1$). Most system identification performed using the hybrid formulation uses the Carpenter-Fridovich model (Ref. 15). Due to the lack of blade motion, inflow and thrust measurements, all derivatives of the inflow and coning equations are usually fixed at their theoretical predictions and only Z_w is estimated.

The hybrid inflow/coning model was applied to ACT/FHS flight test data in (Ref. 11). Due to its bearingless design, the rotor of the ACT/FHS has a relatively large equivalent hinge offset of 10%. Therefore, the coning equation (15) had to be extended to include the influence of hinge offset.

$$\ddot{\beta}_{0} = -\frac{\Omega\gamma}{8} \quad 1 - \frac{8}{3}\varepsilon + \varepsilon^{2} \quad \dot{\beta}_{0}$$

$$-\Omega^{2} \quad 1 + \frac{3\varepsilon}{2(1-\varepsilon)} + \frac{K_{\beta}}{I_{\beta}\Omega^{2}} \quad \beta_{0} \qquad (18)$$

$$-\frac{\Omega\gamma}{6R} \quad 1 - \frac{2}{3}\varepsilon \quad \nu + \frac{\Omega^{2}\gamma}{8} \quad 1 - \frac{4}{3}\varepsilon \quad K_{\theta_{0}}\delta_{col}$$

Furthermore, for the hover case two of the parameters of the hybrid model had to be freed from their analytical predictions to achieve a good match with the flight test data. For the forward flight cases, no modification of the analytical predictions was necessary.

However, when analyzing the identified models, it was discovered that the inclusion of the coning motion led to a high frequency positive transmission zero for the forward flight cases. As can be seen in Fig. 4, the inclusion of coning does not really improve the match of a_z/δ_{col} in forward flight. Therefore, it was decided to drop the coning equations by setting the coefficients corresponding to $\hat{\beta}_0$ to zero in eqs. (13) and (17).

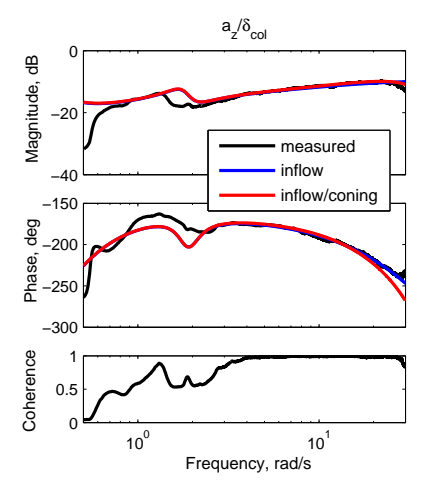


Fig. 4. Match in vertical acceleration for models with and without coning (60 kts)

As it was desired to have the same model structure for all speeds to allow for model stitching, the coning equations were also dropped for the hover case even though this leads to a slight degradation in the match of the frequency response of vertical acceleration due to collective input for frequencies above 12 rad/s (see Fig. 5).

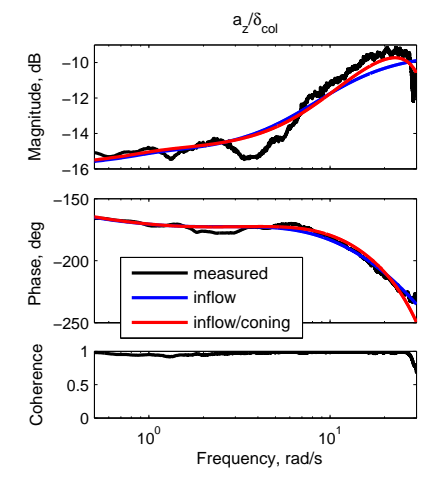


Fig. 5. Match in vertical acceleration for models with and without coning (hover)

REGRESSIVE LEAD-LAG

Simple physical models for the lead-lag dynamics, such as those for the flapping dynamics, are not available. Therefore, a modal approach is usually taken, where two closely spaced complex pole/zero pairs (dipoles) with a common denominator are appended to the pitch and roll rate responses, see (Ref. 13).

Second Order Dipole

A complex (second order) dipole with input u and output y and the transfer function (num = numerator, den = denominator)

$$\frac{y}{u} = \frac{s^2 + 2\zeta_{num}\omega_{num}s + \omega_{num}^2}{s^2 + 2\zeta_{den}\omega_{den}s + \omega_{den}^2}$$
(19)

can be modeled with the state equations

$$\frac{\dot{x}_1}{\dot{x}_2} = \begin{bmatrix} 0 & 1 \\ -\omega_{den}^2 & -2\zeta_{den}\omega_{den} \end{bmatrix} \quad \frac{x_1}{x_2} + \begin{bmatrix} 0 \\ 1 \end{bmatrix} (u) \quad (20)$$

and the output equation

$$y = (\omega_{num}^2 - \omega_{den}^2)x_1 + (2\zeta_{num}\omega_{num} - 2\zeta_{den}\omega_{den})x_2 + u$$
 (21)

Regarding the following transfer function of roll rate (p) due to lateral cyclic input, where the first order quasi-static response is augmented by a second order lead-lag (ll) dipole,

$$\frac{p_{ll}}{\delta_{lat}} = \frac{L_{\delta_{lat}}}{s - L_p} \frac{s^2 + 2\zeta_p \omega_p s + \omega_p^2}{s^2 + 2\zeta_{ll} \omega_{ll} s + \omega_{ll}^2}$$
(22)

it can be interpreted in two ways:

$$\frac{p_{ll}}{\delta_{lat}} = \frac{p}{\delta_{lat}} \frac{p_{ll}}{p} \qquad \text{(dipole at the output)} \tag{23}$$

or

$$\frac{p_{ll}}{\delta_{lat}} = \frac{p_{ll}}{\delta_{lat,ll}} \frac{\delta_{lat,ll}}{\delta_{lat}}$$
 (dipole at the input) (24)

which leads to different state space implementations.

For the first case (dipole at the output), the equations for p/δ_{lat} and the dipole p_{ll}/p (with p as the input) are appended to each other in the state equations

$$\begin{pmatrix} \dot{p} \\ \dot{x}_1 \\ \dot{x}_2 \end{pmatrix} = \begin{bmatrix} L_p & 0 & 0 \\ 0 & 0 & 1 \\ 1 & -\omega_{ll}^2 & -2\zeta_{ll}\omega_{ll} \end{bmatrix} \begin{pmatrix} p \\ x_1 \\ x_2 \end{pmatrix} + \begin{bmatrix} L_{\delta_{lat}} \\ 0 \\ 0 \end{bmatrix} (\delta_{lat})$$
(25)

and the roll rate including lead-lag p_{ll} is calculated by the output equation (see eq. (21))

$$p_{ll} = p + (\omega_p^2 - \omega_{ll}^2)x_1 + (2\zeta_p\omega_p - 2\zeta_{ll}\omega_{ll})x_2$$
 (26)

For the second case (dipole at the input), the input δ_{lat} has to be replaced by $\delta_{lat,ll}$ in the equation for \dot{p}_{ll} . This leads to the following system:

$$\begin{pmatrix} \dot{p}_{ll} \\ \dot{x}_1 \\ \dot{x}_2 \end{pmatrix} = \begin{bmatrix} L_p & L_{x_1} & L_{x_2} \\ 0 & 0 & 1 \\ 0 & -\omega_{ll}^2 & -2\zeta_{ll}\omega_{ll} \end{bmatrix} \begin{pmatrix} p_{ll} \\ x_1 \\ x_2 \end{pmatrix} + \begin{bmatrix} L_{\delta_{lat}} \\ 0 \\ 1 \end{bmatrix} (\delta_{lat})$$

with

$$L_{x_1} = L_{\delta_{lat}}(\omega_p^2 - \omega_{ll}^2) \quad L_{x_2} = L_{\delta_{lat}}(2\zeta_p\omega_p - 2\zeta_{ll}\omega_{ll}) \quad (28)$$

No output equation is required in this case because the transformation from δ_{lat} to $\delta_{lat,ll}$ is already contained in the state equations.

Extension to Two Inputs and Two Outputs

If a second order dipole with the same denominator is also appended to the pitch axis and if both inputs δ_{lon} and δ_{lat} act on p and q, the first formulation with the dipoles at the output leads to state equations

$$\begin{pmatrix}
\dot{p} \\
\dot{q} \\
\dot{x}_{1} \\
\dot{x}_{2} \\
\dot{y}_{1} \\
\dot{y}_{2}
\end{pmatrix} = \begin{bmatrix}
L_{p} & 0 & 0 & 0 & 0 & 0 & 0 \\
0 & M_{q} & 0 & 0 & 0 & 0 & 0 \\
0 & 0 & 0 & 1 & 0 & 0 & 0 \\
1 & 0 & -\omega_{ll}^{2} & -2\zeta_{ll}\omega_{ll} & 0 & 0 & 0 \\
0 & 0 & 0 & 0 & 0 & 1 & 0 \\
0 & 1 & 0 & 0 & -\omega_{ll}^{2} & -2\zeta_{ll}\omega_{ll}
\end{bmatrix}$$

$$\bullet \begin{pmatrix}
p \\
q \\
x_{1} \\
x_{2} \\
y_{1} \\
y_{2}
\end{pmatrix} + \begin{bmatrix}
L_{\delta_{lon}} & L_{\delta_{lat}} \\
M_{\delta_{lon}} & M_{\delta_{lat}} \\
0 & 0 \\
0 & 0 \\
0 & 0
\end{bmatrix}$$

$$\delta_{lon} \\
\delta_{lat} \\
\delta_{lat}$$
(29)

and observation equations

$$p_{ll} = p + (\omega_p^2 - \omega_{ll}^2)x_1 + (2\zeta_p\omega_p - 2\zeta_{ll}\omega_{ll})x_2$$

$$q_{ll} = q + (\omega_q^2 - \omega_{ll}^2)x_1 + (2\zeta_q\omega_q - 2\zeta_{ll}\omega_{ll})x_2$$
(30)

The resulting transfer functions are

$$\frac{p_{ll}}{\delta_{lon}} = \frac{L_{\delta_{lon}}}{s - L_p} \frac{\left[\zeta_p, \omega_p\right]}{\left[\zeta_{ll}, \omega_{ll}\right]} \qquad \frac{p_{ll}}{\delta_{lat}} = \frac{L_{\delta_{lat}}}{s - L_p} \frac{\left[\zeta_p, \omega_p\right]}{\left[\zeta_{ll}, \omega_{ll}\right]}
\frac{q_{ll}}{\delta_{lon}} = \frac{M_{\delta_{lon}}}{s - M_q} \frac{\left[\zeta_q, \omega_q\right]}{\left[\zeta_{ll}, \omega_{ll}\right]} \qquad \frac{q_{ll}}{\delta_{lat}} = \frac{M_{\delta_{lat}}}{s - M_q} \frac{\left[\zeta_q, \omega_q\right]}{\left[\zeta_{ll}, \omega_{ll}\right]}$$
(31)

This means that the dipoles in p_{ll}/δ_{lon} and p_{ll}/δ_{lat} are identical. The same holds for the dipoles in q_{ll}/δ_{lon} and q_{ll}/δ_{lat} .

For the ACT/FHS an alternative approach was used, where two second order dipoles act on the longitudinal and lateral cyclic inputs (Ref. 16). With this modeling variant, different numerator coefficients for all dipoles are possible through

$$\begin{pmatrix} \dot{p}_{ll} \\ \dot{q}_{ll} \\ \dot{x}_{1} \\ \dot{x}_{2} \\ \dot{y}_{1} \\ \dot{y}_{2} \end{pmatrix} = \begin{bmatrix} L_{p} & 0 & L_{x_{1}} & L_{x_{2}} & L_{y_{1}} & L_{y_{2}} \\ 0 & M_{q} & M_{x_{1}} & M_{x_{2}} & M_{y_{1}} & M_{y_{2}} \\ 0 & 0 & 0 & 1 & 0 & 0 \\ 0 & 0 & -\omega_{ll}^{2} & -2\zeta_{ll}\omega_{ll} & 0 & 0 \\ 0 & 0 & 0 & 0 & 0 & 1 \\ 0 & 0 & 0 & 0 & -\omega_{ll}^{2} & -2\zeta_{ll}\omega_{ll} \end{bmatrix}$$

$$\bullet \begin{pmatrix} p_{ll} \\ p_{ll} \\ x_{1} \\ x_{2} \\ y_{1} \\ y_{2} \end{pmatrix} + \begin{bmatrix} L_{\delta_{lon}} & L_{\delta_{lat}} \\ M_{\delta_{lon}} & M_{\delta_{lat}} \\ 0 & 0 \\ 0 & 1 \end{bmatrix} \delta_{lon}$$

$$\delta_{lat}$$

$$\delta_{lon}$$

$$\delta_{lat}$$
(32)

with

$$L_{x_{1}} = L_{\delta_{lon}}(\omega_{xp}^{2} - \omega_{ll}^{2}) \quad L_{x_{2}} = L_{\delta_{lon}}(2\zeta_{xp}\omega_{xp} - 2\zeta_{ll}\omega_{ll})$$

$$L_{y_{1}} = L_{\delta_{lat}}(\omega_{yp}^{2} - \omega_{ll}^{2}) \quad L_{y_{2}} = L_{\delta_{lat}}(2\zeta_{yp}\omega_{yp} - 2\zeta_{ll}\omega_{ll})$$

$$M_{x_{1}} = M_{\delta_{lon}}(\omega_{xq}^{2} - \omega_{ll}^{2}) \quad M_{x_{2}} = M_{\delta_{lon}}(2\zeta_{xq}\omega_{xq} - 2\zeta_{ll}\omega_{ll})$$

$$M_{y_{1}} = M_{\delta_{lat}}(\omega_{yq}^{2} - \omega_{ll}^{2}) \quad M_{y_{2}} = M_{\delta_{lat}}(2\zeta_{yq}\omega_{yq} - 2\zeta_{ll}\omega_{ll})$$

$$(33)$$

The resulting transfer functions are

$$\frac{p_{ll}}{\delta_{lon}} = \frac{L_{\delta_{lon}}}{s - L_p} \frac{\left[\zeta_{xp}, \omega_{xp}\right]}{\left[\zeta_{ll}, \omega_{ll}\right]} \qquad \frac{p_{ll}}{\delta_{lat}} = \frac{L_{\delta_{lat}}}{s - L_p} \frac{\left[\zeta_{yp}, \omega_{yp}\right]}{\left[\zeta_{ll}, \omega_{ll}\right]}
\frac{q_{ll}}{\delta_{lon}} = \frac{M_{\delta_{lon}}}{s - M_q} \frac{\left[\zeta_{xq}, \omega_{xq}\right]}{\left[\zeta_{ll}, \omega_{ll}\right]} \qquad \frac{q_{ll}}{\delta_{lat}} = \frac{M_{\delta_{lat}}}{s - M_q} \frac{\left[\zeta_{yq}, \omega_{yq}\right]}{\left[\zeta_{ll}, \omega_{ll}\right]}$$
(34)

and thus the dipoles in p_{ll}/δ_{lon} and p_{ll}/δ_{lat} have different numerators and are therefore not identical. The same holds for the dipoles in q_{ll}/δ_{lon} and q_{ll}/δ_{lat} .

Fig. 6 shows that the lead-lag dipoles for the ACT/FHS in p/δ_{lon} and p/δ_{lat} are different and can thus only be captured by the model with two dipoles at the inputs and not by the usual formulation with dipoles at the outputs.

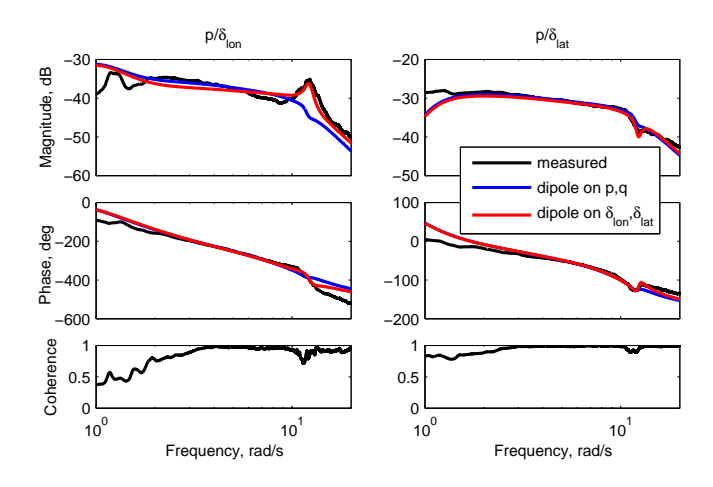


Fig. 6. Match in roll rate due to cyclic inputs for both leadlag models (hover)

Another advantage of the model formulation with the input dipoles is that possible effects of the lead-lag on the longitudinal and lateral accelerations can be captured (see Fig. 7).

On the other hand, the modeling variant with the dipoles on the outputs has the advantage, that the lead-lag influence can also be modeled for collective inputs (see e.g. Fig. 8). For the model with input dipoles, this would require a third dipole and thus two additional state variables.

Formulation with One Second Order Dipole

At DLR, system identification for the ACT/FHS has also been performed using the optimized predictor-based subspace identification (PBSIDopt) method (Ref. 12). This method does not

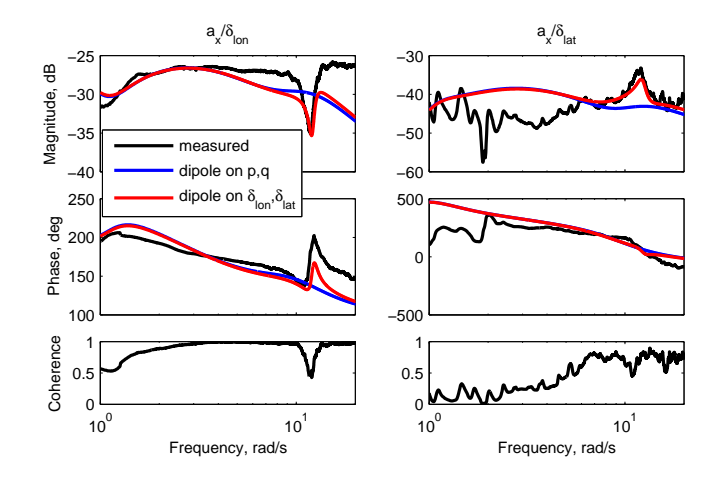


Fig. 7. Match in longitudinal acceleration due to cyclic inputs for both lead-lag models (hover)

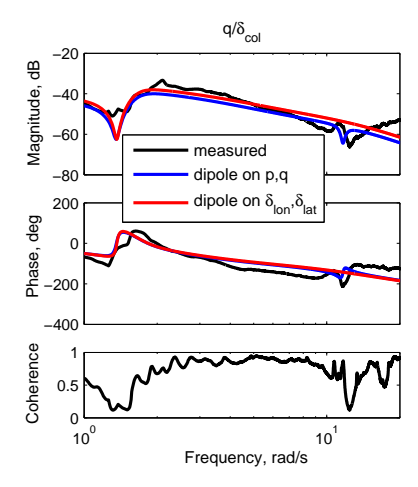


Fig. 8. Match in pitch rate due to collective input for both lead-lag models (30 kts)

require specifying a model structure beforehand but instead the model states are determined along with the corresponding model parameters. The physical interpretation of the resulting models, however, is difficult because the model states cannot be specified and the system matrices are fully populated. Nevertheless, from comparing the eigenvalues of the identified models, it was obvious that the PBSIDopt identified models needed only one dipole to model the regressive lead-lag.

Thus, a new model formulation for the regressive lead-lag was developed where one dipole (with states z_1 and z_2) is triggered by both the longitudinal and lateral cyclic inputs.

$$\begin{pmatrix} \dot{p}_{ll} \\ \dot{q}_{ll} \\ \dot{z}_{1} \\ \dot{z}_{2} \end{pmatrix} = \begin{bmatrix} L_{p} & 0 & L_{z_{1}} & L_{z_{2}} \\ 0 & M_{q} & M_{z_{1}} & M_{z_{2}} \\ 0 & 0 & 0 & 1 \\ 0 & 0 & -\omega_{ll}^{2} & -2\zeta_{ll}\omega_{ll} \end{bmatrix} \begin{pmatrix} p_{ll} \\ p_{ll} \\ z_{1} \\ z_{2} \end{pmatrix} + \begin{bmatrix} L_{\delta_{lon}} & L_{\delta_{lat}} \\ M_{\delta_{lon}} & M_{\delta_{lat}} \\ D_{\delta_{lon}} & D_{\delta_{lat}} \\ 1 & 1 \end{bmatrix} \quad \delta_{lon} \\ \delta_{lat}$$
(35)

This results in the following transfer functions

$$\frac{p_{ll}}{\delta_{lon}} = \frac{1}{s - L_p} \frac{L_{\delta_{lon}} s^2 + P_{x_1} s + P_{x_0}}{[\zeta_{ll}, \omega_{ll}]}$$

$$\frac{p_{ll}}{\delta_{lat}} = \frac{1}{s - L_p} \frac{L_{\delta_{lat}} s^2 + P_{y_1} s + P_{y_0}}{[\zeta_{ll}, \omega_{ll}]}$$

$$\frac{q_{ll}}{\delta_{lon}} = \frac{1}{s - M_q} \frac{M_{\delta_{lon}} s^2 + Q_{x_1} s + Q_{x_0}}{[\zeta_{ll}, \omega_{ll}]}$$

$$\frac{q_{ll}}{\delta_{lat}} = \frac{1}{s - M_q} \frac{M_{\delta_{lat}} s^2 + Q_{y_1} s + Q_{y_0}}{[\zeta_{ll}, \omega_{ll}]}$$
(36)

with

$$\begin{split} P_{x_{1}} &= L_{z_{2}} + L_{z_{1}} D_{\delta_{lon}} + L_{\delta_{lon}} 2\zeta_{ll} \omega_{ll} \\ P_{x_{0}} &= L_{z_{1}} + L_{\delta_{lon}} \omega_{ll}^{2} - L_{z_{2}} D_{\delta_{lon}} \omega_{ll}^{2} + L_{z_{1}} D_{\delta_{lon}} 2\zeta_{ll} \omega_{ll} \\ P_{y_{1}} &= L_{z_{2}} + L_{z_{1}} D_{\delta_{lat}} + L_{\delta_{lat}} 2\zeta_{ll} \omega_{ll} \\ P_{y_{0}} &= L_{z_{1}} + L_{\delta_{lat}} \omega_{ll}^{2} - L_{z_{2}} D_{\delta_{lat}} \omega_{ll}^{2} + L_{z_{1}} D_{\delta_{lat}} 2\zeta_{ll} \omega_{ll} \\ Q_{x_{1}} &= M_{z_{2}} + M_{z_{1}} D_{\delta_{lon}} + M_{\delta_{lon}} 2\zeta_{ll} \omega_{ll} \\ Q_{x_{0}} &= M_{z_{1}} + M_{\delta_{lon}} \omega_{ll}^{2} - M_{z_{2}} D_{\delta_{lon}} \omega_{ll}^{2} + M_{z_{1}} D_{\delta_{lon}} 2\zeta_{ll} \omega_{ll} \\ Q_{y_{1}} &= M_{z_{2}} + M_{z_{1}} D_{\delta_{lat}} + M_{\delta_{lat}} 2\zeta_{ll} \omega_{ll} \\ Q_{y_{0}} &= M_{z_{1}} + M_{\delta_{lat}} \omega_{ll}^{2} - M_{z_{2}} D_{\delta_{lat}} \omega_{ll}^{2} + M_{z_{1}} D_{\delta_{lat}} 2\zeta_{ll} \omega_{ll} \end{split}$$

Again, all dipole numerators are different and thus different dipoles in p_{ll}/δ_{lon} and p_{ll}/δ_{lat} respectively q_{ll}/δ_{lon} and q_{ll}/δ_{lat} can be realized. In the appendix it is shown analytically that the parameters of the two-dipole model can be calculated from those of the one-dipole formulation when the pitch and roll equations are decoupled.

Fig. 9 shows that this one-dipole approach leads to results that are comparable to those obtained with two dipoles at the input.

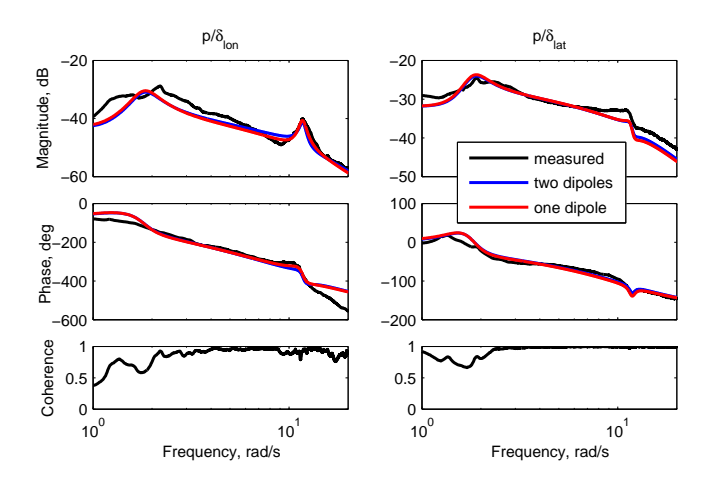


Fig. 9. Match in roll rate due to cyclic inputs for the oneand two-dipole formulations (60 kts)

Furthermore, this one-dipole approach can easily be extended so that the lead-lag is also excited by collective inputs by just adding another column in the control matrix from eq. (35). Thus the one-dipole formulation has the advantages of both of the other two-dipole modeling variants and is simpler because it needs only two lead-lag states.

ENGINE MODELING

After accounting for the rotor degrees of freedom of flapping, inflow and regressive lead-lag, the identified models of the ACT/FHS still had deficits that were attributed to missing engine dynamics. According to (Ref. 13) the effect of the engine/governor dynamics on the fuselage response primarily manifests itself as a large additional phase lag in the p/δ_{col} , q/δ_{col} , and r/δ_{col} frequency responses. In case of the ACT/FHS, deficits were only experienced in the response of yaw rate due to collective input.

Preliminary Investigations

First, it was investigated whether accounting for engine dynamics by a simple lag in the influence of collective input on the angular rates as suggested in (Ref. 13) would be sufficient. For this approach, the time delay in the collective input was approximated by a Padé approximation

$$\frac{\delta_{col}'}{\delta_{col}} = \frac{2/\tau_{en} - s}{2/\tau_{en} + s} \tag{38}$$

where τ_{en} is the time constant. δ_{col} is the original collective input and δ'_{col} the delayed collective input, that is used in the equations of motion for the pitch, roll, and yaw rates. This approach, hovever, did not yield the desired improvement.

Therefore, a linear regression was performed in the time domain using the equation for yaw acceleration

$$\dot{r} = N_r r + N_v v + N_p p + N_{\delta_{col}} \delta_{col} + N_{\delta_{ped}} \delta_{ped} + N_O O + N_O \Omega$$
(39)

The coefficients N_r , ... N_Ω were determined using measured time history data both for the output variable \dot{r} and the inputs r, ..., Ω . This investigation showed that torque Q has a profound influence on the yawing motion whereas no direct influence of rotor speed Ω could be found. Thus, torque modeling with a dynamic engine model was needed.

Frequency Response Modeling

First, the frequency response for rotor speed due to collective was approximated separately. A good approximation was reached with the following model

$$\frac{\Omega}{\delta_{col}} = \frac{K_{\delta_{col}}}{s^2 + 2\zeta_{en}\omega_{en}s + \omega_{en}^2} \frac{s - E_{z,col}}{s - E_p}$$
(40)

which consists of a second order system with frequency ω_{en} and damping ζ_{en} combined by a first order pole/zero pair (dipole) with pole E_p and zero $E_{z,col}$.

In the engine model that was identified for the Firescout UAV (Ref. 13), a second order system for rotor speed is combined with a washout filter modeling the governor dynamics. This washout filter corresponds to setting $E_{z,col}=0$ in eq. (40). The engine of the ACT/FHS is controlled by a FADEC system and

a sufficient approximation of Ω/δ_{col} could only be reached with $E_{z,col} \neq 0$.

Next, the frequency responses due to collective and pedal inputs were approximated with a common denominator. This corresponds to extending eq. (40) by

$$\frac{\Omega}{\delta_{ped}} = \frac{K_{\delta_{ped}}}{s^2 + 2\zeta_{en}\omega_{en}s + \omega_{en}^2} \frac{s - E_{z,ped}}{s - E_p}$$
(41)

Fig. 10 shows the resulting match for two of the five reference speeds. (The drop in coherence around 2 rad/s in Ω/δ_{ped} for the 90 kts case is caused by the influence of dutch roll dynamics.)

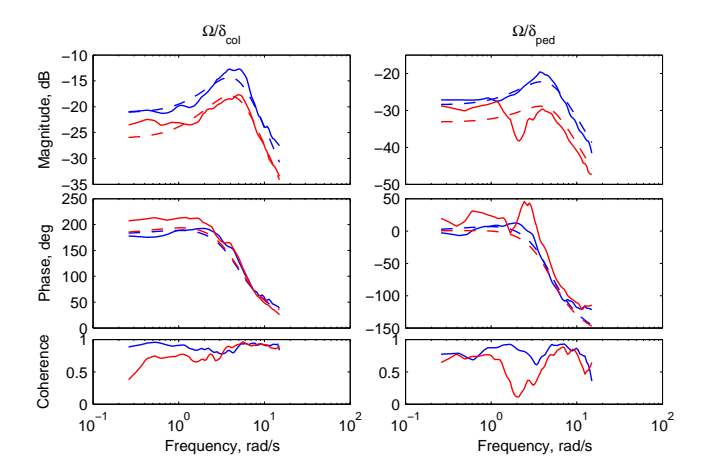


Fig. 10. Transfer function approximation for rotor speed (blue = hover, red = 90 knots, solid = measured, dashed = model)

State Space Model

For inclusion in the identification model, the frequency response models from equations (40) and (41) had to be converted into a state space model. For this, a common zero $E_{z,col} = E_{z,ped} = E_z$ was enforced. Defining an instrumental variable Ω_{en} with

$$\frac{\Omega}{\delta_{col}} = \frac{\Omega}{\Omega_{en}} \frac{\Omega_{en}}{\delta_{col}} = \frac{s - E_z}{s - E_p} \frac{K_{\delta_{col}}}{s^2 + 2\zeta_{en}\omega_{en}s + \omega_{en}^2}$$
(42)

yields the two equations

$$\ddot{\Omega}_{en} = -2\zeta_{en}\omega_{en}\dot{\Omega}_{en} - \omega_{en}^2\Omega_{en} + K_{\delta_{col}}\delta_{col}
\dot{\Omega} = \dot{\Omega}_{en} - E_z\Omega_{en} + E_p\Omega$$
(43)

Adding the pedal input and using matrix notation yields

$$\begin{pmatrix} \ddot{\Omega}_{en} \\ \dot{\Omega}_{en} \\ \dot{\Omega} \end{pmatrix} = \begin{bmatrix} -2\zeta_{en}\omega_{en} & -\omega_{en}^{2} & 0 \\ 1 & 0 & 0 \\ 1 & -E_{z} & E_{p} \end{bmatrix} \begin{pmatrix} \dot{\Omega}_{en} \\ \Omega_{en} \\ \Omega \end{pmatrix} + \begin{bmatrix} K_{\delta_{col}} & K_{\delta_{ped}} \\ 0 & 0 \\ 0 & 0 \end{bmatrix} \begin{pmatrix} \delta_{col} \\ \delta_{ped} \end{pmatrix}$$

$$(44)$$

Tischler (Ref. 13) suggests using a Taylor series for modeling the torque dynamics

$$\dot{Q} = R_Q Q + R_{\Omega} \Omega + R_{\dot{\Omega}} \dot{\Omega} + R_{\delta_{col}} \delta_{col} + R_{\delta_{ned}} \delta_{ped}$$
 (45)

Inserting the equations for $\dot{\Omega}$ from eq. (43) yields

$$\dot{Q} = R_{\dot{\Omega}} \dot{\Omega}_{en} - E_z R_{\dot{\Omega}} \Omega_{en} + (R_{\Omega} + E_p R_{\dot{\Omega}}) \Omega + R_Q Q
+ R_{\delta_{col}} \delta_{col} + R_{\delta_{ned}} \delta_{ped}$$
(46)

This equations was added to the system from eq. (44) to arrive at the desired state space system for rotor speed and torque.

$$\begin{pmatrix} \ddot{\Omega}_{en} \\ \dot{\Omega}_{en} \\ \dot{\Omega} \\ \dot{Q} \end{pmatrix} = \begin{bmatrix} -2\zeta_{en}\omega_{en} & -\omega_{en}^{2} & 0 & 0 \\ 1 & 0 & 0 & 0 \\ 1 & -E_{z} & E_{p} & 0 \\ R_{\dot{\Omega}} & -E_{z}R_{\dot{\Omega}} & R_{\Omega} + E_{p}R_{\dot{\Omega}} & R_{Q} \end{bmatrix} \begin{pmatrix} \dot{\Omega}_{en} \\ \Omega_{en} \\ \Omega \\ Q \end{pmatrix} + \begin{bmatrix} K_{\delta_{col}} & K_{\delta_{ped}} \\ 0 & 0 \\ 0 & 0 \\ R_{\delta_{col}} & R_{\delta_{ped}} \end{bmatrix} \begin{pmatrix} \delta_{col} \\ \delta_{ped} \end{pmatrix}$$

$$(47)$$

The parameters of this model were identified for each of the five reference speeds with the maximum likelihood (ML) frequency domain method using collective and pedal sweep maneuvers. The parameter R_{Ω} exhibited high uncertainty and was thus set to zero. The identified models were validated with 3211-multistep maneuvers. Fig. 11 shows that the match in torque and rotor speed both for collective and pedal inputs in hover is quite good.

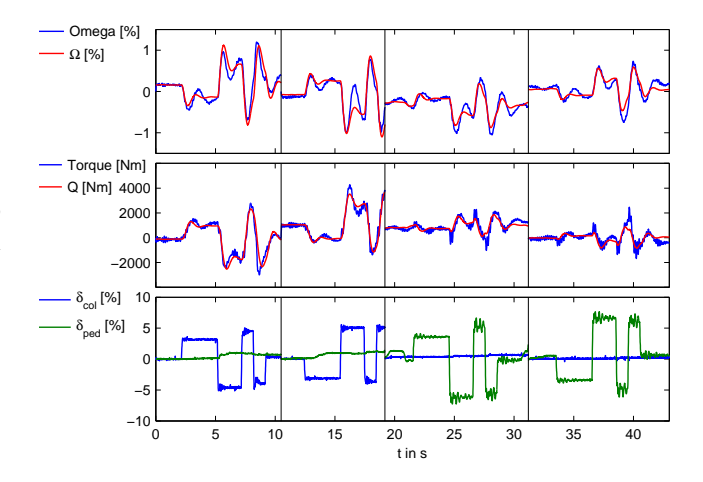


Fig. 11. Validation of the identified engine model in hover (blue, green = measured, red = model)

Model Simplifications

Before the development of the models described in this paper, corrections in transfer function form had been used to reduce the remaining model deficits of the prior models (Ref. 17). As the corrections to r/δ_{col} , which were needed to account for the

missing engine dynamics, used the same transfer function for all speeds, it was tried to simplify the identified engine model accordingly.

First the calculation of torque from rotor speed was investigated by using the measured data for Ω and $\dot{\Omega}$ in eq. (45). This showed that the relationship between rotor speed and torque does not vary with speed. Also, the pedal influence coefficient $R_{\delta_{ped}}$ could be neglected.

Next, it was tried to simplify the rotor speed model. As the frequency responses from collective and pedal to Ω have a similar shape for all speeds and mainly a different amplitude (see Fig. 10), a model for rotor speed was determined where the parameters ζ_{en} , ω_{en} , E_z and E_p are identical for all speeds and only the control derivatives $K_{\delta_{col}}$ and $K_{\delta_{ped}}$ are different (see eq. (44)). The match of this simplified model was almost as good as for the models that had been optimized separately for each reference speed.

Model Integration

Finally, the identified engine model was coupled to the overall model. Fig. 12 shows the match in the frequency responses r/δ_{ped} and r/δ_{col} in hover for the models with and without engine modeling. As expected, the yaw rate response to collective input improves both in amplitude and in phase. Interestingly enough, the yaw response to pedal inputs (on-axis response) improves also.

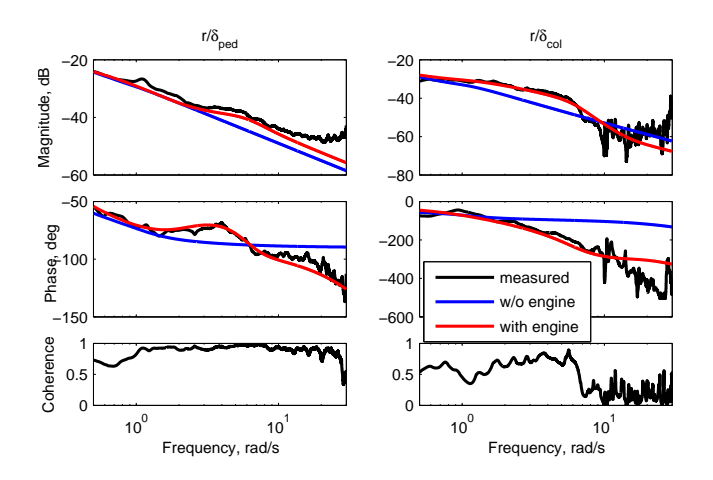


Fig. 12. Improvement of yaw responses by engine modeling (hover)

INTEGRATED MODEL

The overall models including rotor and engine dynamics were identified in an incremental way. The ML frequency domain method was used for all state space model identification.

First, 6-DoF models were identified over the frequency range of 0.1-10 rad/s. Next, the flapping dynamics were added using the modified explicit formulation as described in this paper. The theoretical prediction from eq. (4) was used as a

starting value for the flapping time constant and the frequency range for the approximation was extended to 0.5-15 rad/s. To extend the model range of validity even further, the explicit inflow equations were then added to the model and all model parameters optimized for a frequency range of 0.5-30 rad/s.

To allow for model stitching, care was taken in every step, that it would be possible to interpolate between the models identified for each of the five reference speeds. Fig. 13 shows the identified moment derivatives versus speed. It can be seen that the models for the different reference speeds have similar sets of free parameters and that the change over speed for all derivatives is smooth.

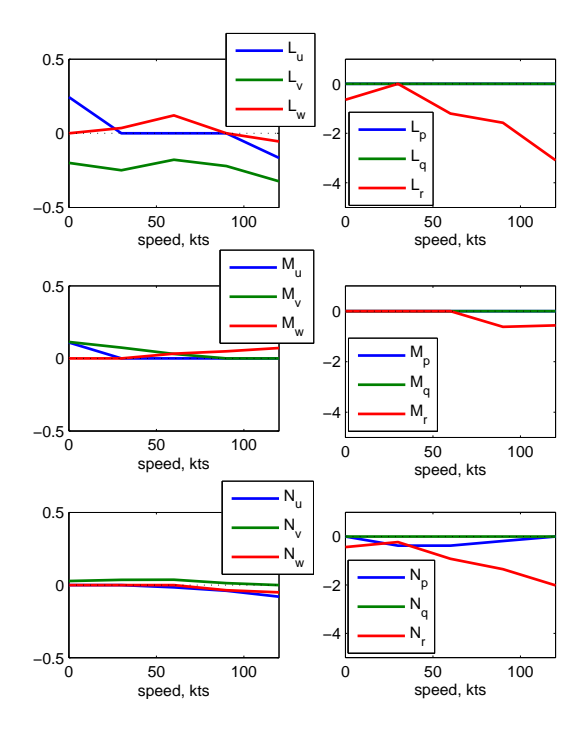


Fig. 13. Identified moment derivatives versus speed

Next, the engine dynamics were added. For this step, the engine model parameters were fixed at the identified values from the separate engine model identification. Coupling derivatives N_Q and L_Q (the latter only for hover and low speed) were introduced and estimated together with fuselage and rotor derivatives over a frequency range of 0.5-30 rad/s.

For the ACT/FHS the influence of the regressive lead-lag mode is only a very local effect around 12 rad/s (see Figs. 6 and 7) and thus could be identified last. The one-dipole formulation was used and extending it to collective inputs was not necessary because the lead-lag influence on the angular rates due to collective input is not significant throughout the flight envelope. For this step, all model parameters determined so far were fixed and only the lead-lag model parameters were identified over a frequency range of 10-15 rad/s. Finally, the identified lead-lag parameters were fixed and the remaining parameters re-iterated over the full frequency range.

Figure 14 illustrates the achieved frequency domain match of the hover model. The models for the forward flight cases are of similar quality.

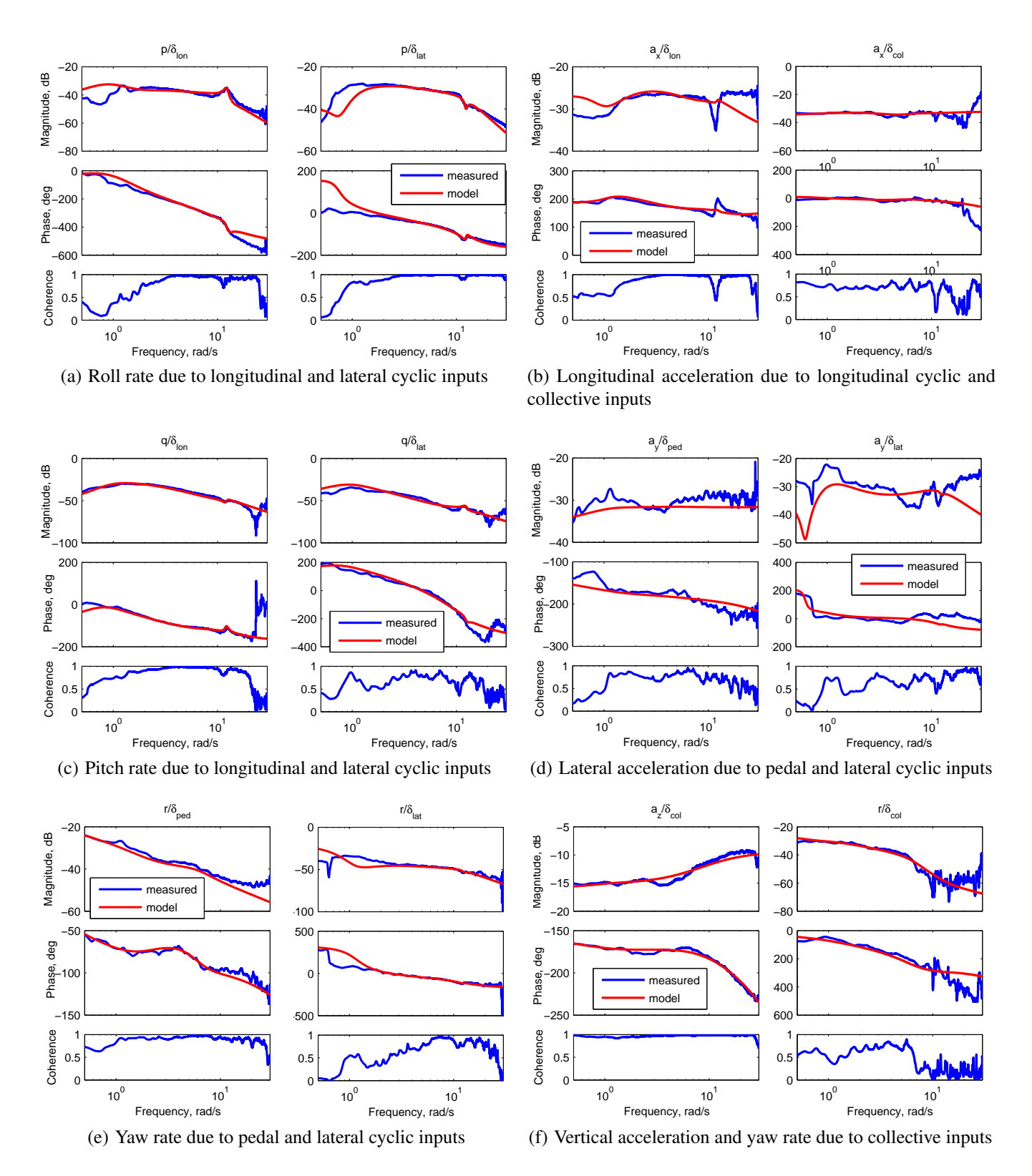


Fig. 14. Match of the overall model in hover

Some modeling deficits can still be seen where a rising amplitude in the frequency range of 20-30 rad/s is not covered by the model, see for example r/δ_{ped} in Fig. 14(e) or a_x/δ_{col} in Fig. 14(b). These deficites are attributed to structural modes such as tailboom flexibility and will be accounted for in the future.

CONCLUSIONS

System identification was used to generate models for the ACT/FHS helicopter that fulfill the following requirements:

- The models should be accurate for frequencies up to 30 rad/s.
- It must be possible to interpolate between the models for the five reference speeds.
- The models have to be invertible with respect to the output variables p, q, r, a_z and thus the corresponding submodels must not have any positive transmission zeros.

To arrive at this goal, the following submodel improvements were necessary:

- 1. Using collective control as an input to the flapping angles avoided positive transmission zeroes in the explicit flapping modeling.
- 2. In the modeling of the vertical axis coning had to be neglected as it caused positive transmission zeros for the forward flight cases.
- A new modeling variant for the regressive lead-lag was developed that needs only one second order dipole (two states).
- 4. Integrating a seperately developed engine model improved the yaw rate response, especially in hover.

Models with this extended structure were identified for five reference speeds and form the basis for a quasi-nonlinear simulation and for control law development.

Author contact: Susanne Seher-Weiß, susanne.seher-weiss@dlr.de

APPENDIX

Relationship Between One-Dipole and Two-Dipole Formulation

The relationship between the lead-lag formulation with two dipoles acting on the inputs and the model with only one dipole that is triggered by both the longitudinal and the lateral cyclic input can be derived by comparing the numerator coefficients in the transfer functions from eqs. (34) and (36).

The coefficients for s^2 are $L_{\delta_{lon}}$ and $L_{\delta_{lat}}$ respectively $M_{\delta_{lon}}$ and $M_{\delta_{lat}}$ for both models which means that the control derivatives for both models are identical.

Comparing the coefficients for s^1 and taking into account the eqs. (33) and (37) for the model coefficients yields

$$L_{x_{2}} = L_{\delta_{lon}} (2\zeta_{xp}\omega_{xp} - 2\zeta_{ll}\omega_{ll}) = L_{z_{2}} + L_{z_{1}}D_{\delta_{lon}}$$

$$L_{y_{2}} = L_{\delta_{lat}} (2\zeta_{yp}\omega_{yp} - 2\zeta_{ll}\omega_{ll}) = L_{z_{2}} + L_{z_{1}}D_{\delta_{lat}}$$

$$M_{x_{2}} = M_{\delta_{lon}} (2\zeta_{xq}\omega_{xq} - 2\zeta_{ll}\omega_{ll}) = M_{z_{2}} + M_{z_{1}}D_{\delta_{lon}}$$

$$M_{y_{2}} = M_{\delta_{lon}} (2\zeta_{yq}\omega_{yq} - 2\zeta_{ll}\omega_{ll}) = M_{z_{2}} + M_{z_{1}}D_{\delta_{lon}}$$

$$(48)$$

Similarly, comparing the coefficients for s^0 yields

$$L_{x_{1}} = L_{\delta_{lon}}(\omega_{xp}^{2} - \omega_{ll}^{2})$$

$$= L_{z_{1}} - L_{z_{2}}D_{\delta_{lon}}\omega_{ll}^{2} + L_{z_{1}}D_{\delta_{lon}}2\zeta_{ll}\omega_{ll}$$

$$L_{y_{2}} = L_{\delta_{lat}}(\omega_{yp}^{2} - \omega_{ll}^{2})$$

$$= L_{z_{1}} - L_{z_{2}}D_{\delta_{lat}}\omega_{ll}^{2} + L_{z_{1}}D_{\delta_{lat}}2\zeta_{ll}\omega_{ll}$$

$$M_{x_{2}} = M_{\delta_{lon}}(\omega_{xq}^{2} - \omega_{ll}^{2})$$

$$= M_{z_{1}} - M_{z_{2}}D_{\delta_{lon}}\omega_{ll}^{2} + M_{z_{1}}D_{\delta_{lon}}2\zeta_{ll}\omega_{ll}$$

$$M_{y_{2}} = M_{\delta_{lat}}(\omega_{yq}^{2} - \omega_{ll}^{2})$$

$$= M_{z_{1}} - M_{z_{2}}D_{\delta_{lon}}\omega_{ll}^{2} + M_{z_{1}}D_{\delta_{lon}}2\zeta_{ll}\omega_{ll}$$

$$= M_{z_{1}} - M_{z_{2}}D_{\delta_{lon}}\omega_{ll}^{2} + M_{z_{1}}D_{\delta_{lon}}2\zeta_{ll}\omega_{ll}$$

This shows that the coefficients of the two-dipole formulation can be calculated from those for the one-dipole version.

For the reverse relationship, subtracting the first and second equation from (48) yields

$$L_{x_2} - L_{y_2} = L_{z_1} (D_{\delta_{lon}} - D_{\delta_{lat}})$$
 (50)

Multiplying the first equation from (48) by $-D_{\delta_{lat}}$ and adding the second equation multiplied by $D_{\delta_{lan}}$ gives

$$D_{\delta_{lon}}L_{y_2} - D_{\delta_{lat}}L_{x_2} = L_{z_2}(D_{\delta_{lon}} - D_{\delta_{lat}})$$
 (51)

Similarly, subtracting the first and second equation from (49) yields

$$L_{x_1} - L_{y_1} = L_{z_1} (D_{\delta_{lon}} - D_{\delta_{lat}}) 2\zeta_{ll} \omega_{ll} - L_{z_2} (D_{\delta_{lon}} - D_{\delta_{lat}}) \omega_{ll}^2$$
(52)

and multiplying the first equation from (49) by $-D_{\delta_{lat}}$ and adding the second equation multiplied by $D_{\delta_{lan}}$ gives

$$D_{\delta_{lon}}L_{y_1} - D_{\delta_{lat}}L_{x_1} = L_{z_1}(D_{\delta_{lon}} - D_{\delta_{lat}})$$
 (53)

Inserting eqs. (50) and (51) into eq. (52) yields

$$L_{x_1} - L_{y_1} = (D_{\delta_{lon}} L_{y_2} - D_{\delta_{lat}} L_{x_2}) \omega_{ll}^2 + (L_{x_2} - L_{y_2}) 2\zeta_{ll} \omega_{ll}$$
(54)

or

$$(D_{\delta_{lon}}L_{y_2} - D_{\delta_{lat}}L_{x_2})\omega_{ll}^2 = L_{x_1} - L_{y_1} + (L_{x_2} - L_{y_2})2\zeta_{ll}\omega_{ll}$$
(55)

and combining eqs. (50) and (53) gives

$$L_{x_2} - L_{y_2} = D_{\delta_{lor}} L_{y_1} - D_{\delta_{lor}} L_{x_1}$$
 (56)

Now that L_{z_1} and L_{z_2} have been eliminated, $D_{\delta_{lon}}$ and $D_{\delta_{lat}}$ can be separated by multiplying eq. (55) by L_{x_1} and subtracting eq. (56) multiplied by $L_{x_2} \omega_{ll}^2$

$$D_{\delta_{lon}}(L_{x_1}L_{y_2} - L_{x_2}L_{y_1})\omega_{ll}^2$$

$$= L_{x_1}(L_{x_1} - L_{y_1}) + L_{x_1}(L_{x_2} - L_{y_2})2\zeta_{ll}\omega_{ll} \qquad (57)$$

$$-L_{x_2}(L_{x_2} - L_{y_2})\omega_{ll}^2$$

and multiplying eq. (55) by L_{y_1} and subtracting eq. (56) multiplied by L_{y_2} yields

$$D_{\delta_{lat}}(L_{x_1}L_{y_2} - L_{x_2}L_{y_1})\omega_{ll}^2$$

$$= L_{y_1}(L_{x_1} - L_{y_1}) + L_{y_1}(L_{x_2} - L_{y_2})2\zeta_{ll}\omega_{ll} \qquad (58)$$

$$-L_{y_2}(L_{x_2} - L_{y_2})\omega_{ll}^2$$

Eqs. (57) and (58) allow to determine $D_{\delta_{lon}}$ and $D_{\delta_{lat}}$ from the coefficients of the two-dipole model. Inserting the results into eqs. (50) and (51) then yields L_{z_1} and L_{z_2} .

So far, only the coefficients of the roll rate transfer functions have been used. Analogously, $D_{\delta_{lon}}$ and $D_{\delta_{lat}}$ can also be determined from the coefficients of the pitch equations. This leads to a constraint for the coefficients of the two-dipole formulation. Thus, the two model formulations are not fully equivalent.

REFERENCES

¹von Grünhagen, W., Schönenberg, T., Lantzsch, R., Lusardi, J. A., Lee, D., and Fischer, H., "Handling qualities studies into the interaction between active sidestick parameters and helicopter response types," *CEAS Aeronautical Journal*, Vol. 5, (1), 2014, pp. 13–28.

doi: 10.1007/s13272-013-0079-7

²Greiser, S., Lantzsch, R., Wolfram, J., Wartmann, J., Müllhäuser, M., Lüken, T., Döhler, H.-U., and Peinecke, N., "Results of the pilot assistance system Assisted Low-Level Flight and Landing on Unprepared Landing Sites obtained with the ACT/FHS research rotorcraft," *Aerospace Science and Technology*, Vol. 45, September 2015, pp. 215227. doi: 10.1016/j.ast.2015.05.017

³Kim, H.-M., Nonnenmacher, D., Götz, J., Weber, P., von Hinüber, E., and Knedlik, S., "Initial flight tests of an automatic slung load control system for the ACT/FHS," *CEAS Aeronautical Journal*, Vol. 7, (2), 2016, pp. 209–224. doi: 10.1007/s13272-016-0181-8

⁴Seher-Weiß, S. and von Grünhagen, W., "EC 135 System Identification for Model Following Control and Turbulence Modeling," 1st CEAS European Air and Space Conference, CEAS-2007-275, September 2007.

⁵Greiser, S. and Seher-Weiß, S., "A contribution to the development of a full flight envelope quasi-nonlinear helicopter simulation," *CEAS Aeronautical Journal*, Vol. 5, (1), 2014, pp. 53–66.

doi: 10.1007/s13272-013-0090-z

⁶Zivan, L. and Tischler, M. B., "Development of a Full Flight Envelope Helicopter Simulation Using System Identification," *J. Am. Helicopter Soc*, Vol. 55, (2), 2010, pp. 022003–1–022003–15.

doi: 10.4050/JAHS.55.022003

⁷Tobias, E. L., Tischler, M. B., Berger, T., and Hagerott, S. G., "Full Flight-Envelope Simulation and Piloted Fidelity Assessment of a Business Jet Using a Model Stitching Architecture," AIAA SciTech, Modeling and Simulation Technologies Conference, January 2015.

⁸Mansur, M. H. and Tischler, M. B., "Flight Test Comparison of Alternate Strategies for Multi-Loop Control Law Optimization," AHS 69th Annual Forum, May 2013.

⁹Wartmann, J., "Model validation and analysis using feedforward control flight test data," *CEAS Aeronautical Journal*, Vol. 6, (3), 2015, pp. 429439.

doi: 10.1007/s13272-015-0152-5

¹⁰Seher-Weiß, S. and von Grünhagen, W., "Comparing explicit and implicit modeling of rotor flapping dynamics for the EC 135," *CEAS Aeronautical Journal*, Vol. 5, (3), 2014, pp. 319332.

doi: 10.1007/s13272-014-0109-0

¹¹Seher-Weiß, S., "Comparing different approaches for modeling the vertical motion of the EC 135," *CEAS Aeronautical Journal*, Vol. 6, (3), 2015, pp. 395406.

doi: 10.1007/s13272-014-0109-0

¹²Wartmann, J. and Seher-Weiß, S., "Application of the Predictor-Based Subspace Identification Method to Rotorcraft System Identification," 39th European Rotorcraft Forum, September 2013.

¹³Tischler, M. B. and Remple, R. K., *Aircraft and Rotorcraft System Identification: Engineering Methods with Flight-Test Examples*, American Institute of Aeronautics and Astronautics, Inc., Reston, VA, second edition, chapter 15, 2012.

¹⁴Chen, R. T. and Hindson, W. S., "Influence of Dynamic Inflow on the Helicopter Vertical Response," Technical Report NASA TM 88327, June 1986.

¹⁵Tischler, M. B. and Tomashofski, C. A., "Flight Test Identification of SH-2G Flapped-Rotor Helicopter Flight Mechanics Models," *J. Am. Helicopter Soc*, Vol. 47, (1), 2002, pp. 18–32.

¹⁶Seher-Weiß, S. and von Grünhagen, W., "Development of EC 135 turbulence models via system identification," *Aerospace Science and Technology*, Vol. 23, December 2012, pp. 4352.

doi: 10.1016/j.ast.2011.09.008

¹⁷Greiser, S. and von Grünhagen, W., "Improving System Identification Results: Combining a Physics-Based Stitched Model with Transfer Function Models Obtained Through Inverse Simulation," AHS 72nd Annual Forum, May 2016.